Full-Wave Analysis of Quasi-Optical Structures

Todd W. Nuteson, *Student Member, IEEE*, Gregory P. Monahan, *Member, IEEE*, Michael B. Steer, *Senior Member, IEEE*, Krishna Naishadham, *Member, IEEE*, James W. Mink, *Fellow, IEEE*, Konstantin K. Kojucharow, and James Harvey, *Member, IEEE*

***Abstract*—A full-wave moment method implementation, using a combination of spatial and spectral domains, is developed for the analysis of quasi-optical systems. An electric field dyadic Green's function, including resonant and nonresonant terms corresponding to coupling from modal and nonmodal fields, is employed in a Galerkin routine. The dyadic Green's function is derived by separately considering paraxial and nonparaxial fields and is much easier to develop than a mixed, scalar and vector, potential Green's function. The driving point impedance of several antenna elements in a quasi-optical open cavity resonator and a 3 × 3 grid in free space are computed and compared with measurements.**

I. Introduction

QUASI-OPTICAL power combining techniques provide a means for combining power from numerous solid-state millimeter-wave sources attached to radiating elements such as antenna arrays or grids, as shown in Figs. 1 and 2. The power from the radiating elements is combined in free-space over a distance of many wavelengths to channel power predominately into a single paraxial mode. The complex device field interactions render it difficult to optimize efficiencies and ensure stable operation. However, computer aided analysis techniques are evolving to aid in design. The strategy is to develop, using numerical field analysis, a multiport impedance model of the linear part of the quasi-optical system. This can then be interfaced with commercial microwave circuit simulators. Efficiency requires that volumetric discretization must be avoided. By utilizing Green's functions appropriate to the physical structure, discretization can be limited to surfaces. In [1]–[4] a series of developments culminated in a straight forward methodology for developing the dyadic Green's function of a quasi-optical structure. The dyadic Green's function is derived by separately considering paraxial and nonparaxial fields. It is not feasible to derive a mixed, scalar and vector, potential Green's function, as required in conventional space domain moment method techniques. As an alternative, we have adapted an efficient moment method field solver [5], [6] to use dyadic Green's functions.

Manuscript received June 16, 1995; revised January 17, 1996. This work was supported in part by the U.S. Army Research Office through Grants DAAL03-89-D-0030 and DAAH04-95-1-0536 and by subcontract from Scientific Research Associated, Inc. under U.S. Army Missile Command Contract DAAH01-95-C-R111.

T. W. Nuteson, G. P. Monahan, M. B. Steer, and J. W. Mink are with the Electronics Research Laboratory, Department of Electrical and Computer Engineering, North Carolina State University, Raleigh, NC 27695-7911 USA.

K. Naishadham is with the Department of Electrical Engineering, Wright State University, Dayton, OH 45435 USA.

K. K. Kojucharow is with the Department of Electrical and Computer Engineering, University of Technology, Dresden, Germany.

J. Harvey is with the U.S. Army Research Office, Research Triangle Park, NC 27709-2211 USA.

Publisher Item Identifier S 0018-9480(96)03037-2.

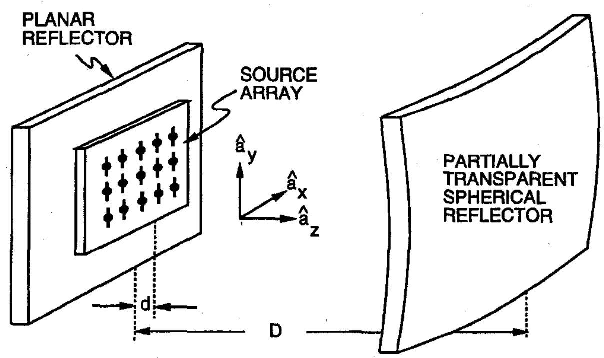

Fig. 1. A quasi-optical power combiner configuration for an open cavity resonator.

The modeling of quasi-optical systems has generally been based on the unit cell approach [7], [8] where the minimum three dimensional cell of an array, generally containing a single active device, is modeled using symmetry of the structure to establish electrical and magnetic side-walls for the cell. A moment method or finite element program is then used to electrically characterize the cell and obtain the impedance presented to a single device. The unit cell approach assumes an infinitely periodic structure with no mutual coupling. In order to obtain accurate modeling, structures of finite extent must be considered along with mutual coupling. In this paper we introduce a moment method technique [9] using a dyadic Green's function which describes all of the electric fields, including paraxial and nonparaxial fields, for radiating elements of finite size in an open cavity resonator and for a 3 × 3 grid in free space. Mutual coupling from all of the elements in the quasi-optical systems are considered.

II. Open Cavity Resonator Dyadic Green's Function

A. General Description

A dyadic Green's function for the plano-concave quasi-optical open cavity resonator was developed by Heron *et al.* [2]–[4]. The cavity resonator, shown in Fig. 1, consists of a planar reflector at $z = 0$ and a partially transmitting spherical reflector with its center located at $z = D$. The planar reflector is assumed to be perfectly conducting with infinite dimensions in the transverse direction and the spherical reflector is of finite dimension with focal length with respect to the x and y axis, F_x and F_y, respectively. The medium in the cavity is free space. The electric field dyadic Green's function of the open cavity resonator is derived in two parts [3], [4]

$$\bar{\bar{\mathbf{G}}}_E = \bar{\bar{\mathbf{G}}}_{En} + \bar{\bar{\mathbf{G}}}_{Er} \qquad (1)$$

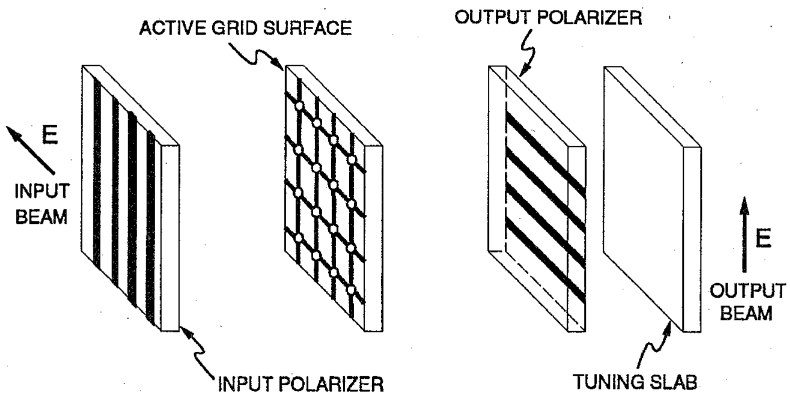

Fig. 2. A grid amplifier on a dielectric slab with X and Y polarizers.

where $\bar{\bar{\mathbf{G}}}_{Er}$ describes the effect of the resonator (cavity) modal fields and $\bar{\bar{\mathbf{G}}}_{En}$ describes the nonresonator fields. The nonresonator fields are found by removing the paraxial component $\bar{\bar{\mathbf{G}}}_{Ep}$ from the half-space Green's function, $\bar{\bar{\mathbf{G}}}_{Eh}$, to give

$$\bar{\bar{\mathbf{G}}}_E = \bar{\bar{\mathbf{G}}}_{Eh} - \bar{\bar{\mathbf{G}}}_{Ep} + \bar{\bar{\mathbf{G}}}_{Er}. \tag{2}$$

The Green's function is evaluated in two parts

$$\bar{\bar{\mathbf{G}}}_E = \bar{\bar{\mathbf{G}}}_{Ec} + \bar{\bar{\mathbf{G}}}_{Eh} \tag{3}$$

where $\bar{\bar{\mathbf{G}}}_{Ec} = \bar{\bar{\mathbf{G}}}_{Er} - \bar{\bar{\mathbf{G}}}_{Ep}$ represents the cavity contribution of the open cavity resonator and $\bar{\bar{\mathbf{G}}}_{Eh}$ represents the half-space (direct radiation) contribution. However $\bar{\bar{\mathbf{G}}}_{Eh}$, as presented in [3], is not suitable for inclusion in a moment method field solver because of numerical problems. We develop here a half-space dyadic Green's function in the spectral domain which has both the required numerical stability and compatibility with the cavity dyadic Green's function. The development of $\bar{\bar{\mathbf{G}}}_{Ec}$ is based on that described in [2].

B. Cavity Contribution

The cavity resonant dyadic Green's function $\bar{\bar{\mathbf{G}}}_{Er}$ describes the coupling between an electric current source, located on the plane $z = d$, and the cavity modal fields in the cavity whereas the paraxial dyadic Green's function $\bar{\bar{\mathbf{G}}}_{Ep}$ describes the paraxial propagation due to the traveling wave-beams in the absence of the spherical reflector. With the subtraction of the paraxial components from the resonator components, the dyadic Green's function, for the range $0 < z < D$, is given by [3]

$$\bar{\bar{\mathbf{G}}}_{Ec} = -\sum_{m=0}^{N_m}\sum_{n=0}^{N_n} \frac{R_{mn}\psi_{mn}}{2(1+R_{mn}\psi_{mn})} \cdot \left(E_{mn}^{-} - E_{mn}^{+}\right)\left(E_{mn}^{\prime -} - E_{mn}^{\prime +}\right)\bar{\bar{\mathbf{I}}}_t \tag{4}$$

where N_m and N_n represent the number of transverse modes and $\bar{\bar{\mathbf{I}}}_t = \hat{\mathbf{a}}_x\hat{\mathbf{a}}_x + \hat{\mathbf{a}}_y\hat{\mathbf{a}}_y$ is the unit transverse dyad. Primed coordinates denote the source location and unprimed coordinates denote the test location. The terms R_{mn} and ψ_{mn} represent the reflection coefficient and phase, respectively, of the traveling wave-beam modes. The scalar electric modal field E_{mn} is given by the Hermite-Gaussian traveling wave-beam as [10]

$$\begin{aligned} E_{mn}^{\pm}&(x,y,z) \\ &= \sqrt{\frac{Z_0}{\pi \bar{X}\bar{Y} m! n!}}(1+u^2)^{-1/4}(1+v^2)^{-1/4} \\ &\cdot He_m(\sqrt{2}x/x_z)He_n(\sqrt{2}y/y_z) \\ &\cdot \exp\left\{-\frac{1}{2}[(x/x_z)^2 + (y/y_z)^2] \right. \\ &\qquad \mp j\left[k_0 z + \frac{1}{2}(u(x/x_z)^2 + v(y/y_z)^2) \right. \\ &\qquad\qquad - \left(m+\frac{1}{2}\right)\tan^{-1}(u) \\ &\qquad\qquad \left.\left. - \left(n+\frac{1}{2}\right)\tan^{-1}(v)\right]\right\} \end{aligned} \tag{5}$$

where

$$u = \frac{z}{k_0\bar{X}^2}, \qquad v = \frac{z}{k_0\bar{Y}^2}$$
$$x_z^2 = \bar{X}^2(1+u^2), \quad y_z^2 = \bar{Y}^2(1+v^2)$$

with the Gaussian mode parameters defined as [10]

$$\bar{X}^2 = \frac{1}{k_0}\sqrt{F_x D\left(2 - \frac{D}{F_x}\right)} \tag{6}$$

$$\bar{Y}^2 = \frac{1}{k_0}\sqrt{F_y D\left(2 - \frac{D}{F_y}\right)}. \tag{7}$$

The Gaussian mode parameters $\bar{X}$ and $\bar{Y}$ determine the rate at which the field strength decays in the $\hat{\mathbf{a}}_x$ and $\hat{\mathbf{a}}_y$ directions respectively. In the above expressions Z_0 and k_0 represent the free space impedance and wavenumber, respectively, given by

$$Z_0 = \sqrt{\frac{\mu_0}{\epsilon_0}}, \quad k_0 = \omega\sqrt{\mu_0\epsilon_0}.$$

The Hermite polynomials, defined in [11]

$$He_n(x) = (-1)^n \exp(x^2/2)\frac{d^n}{dx^n}\left[\exp(-x^2/2)\right] \tag{8}$$

are orthogonal functions. The $E_{mn}^{\pm}$ fields represent the desired wave-beam modes with the beam waist at $z = 0$. E_{mn}^{+}

refers to propagation in the positive $\hat{\mathbf{a}}_z$ direction and E_{mn}^- in the negative $\hat{\mathbf{a}}_z$ direction. An assumption is made that the electric field has only transverse components and no $\hat{\mathbf{a}}_z$ component (quasi-TEM modes). This assumption is valid since the spherical reflector has a radius of curvature much greater than the wavelength of operation. This approximation holds true especially near $z = 0$ where the phase front is flat and the fields are purely transverse. The antennas are sufficiently close to $z = 0$ $(d \ll D)$ that the fields are approximately TEM.

The phase term ψ_{mn} is the ratio, for the mnth mode, of the intensity for each mode of the outgoing wave-beam to the incoming wave-beam evaluated at the spherical reflector surface, $z = D$, given as

$$\psi_{mn} = \frac{E_{mn}^+(x, y, D)}{E_{mn}^-(x, y, D)}. \tag{9}$$

A good approximation for ψ_{mn} can be found by evaluating (9) at $x = y = 0$. At resonance, the phase of the traveling wave-beam should remain unchanged after one complete pass through the resonator so that the resonant frequency for each cavity mode occurs when the product $R_{mn}\psi_{mn}$ in the cavity Green's function (4) approaches -1. For an mn transverse family there is an infinite number of resonant frequencies which we will index by q where q is the number of half wavelengths along the cavity axis. Thus the field structure in the cavity can be designated fully as $\mathrm{TEM}_{m,n,q}$.

C. Cavity Losses

For the open cavity resonator two types of losses are considered, conductor and diffraction losses which are due to the finite conductivity and aperture size of the spherical reflector, respectively. With the combination of these losses, the modal value for R_{mn} can be found as

$$R_{mn} = -|\Gamma|\alpha_{d,mn} \tag{10}$$

where Γ represents conductor losses and $\alpha_{d,mn}$ represents diffraction losses and power extracted from the cavity. The reader is referred to [2] for techniques for the evaluation of (10).

D. Half-Space Green's Function

The half-space is defined to be the region, $z > 0$, with the absence of the spherical reflector. A dyadic Green's function in the spatial domain for this geometry is given in [12] as

$$\bar{\bar{\mathbf{G}}}_{Eh}(\mathbf{r} \mid \mathbf{r}') = j\omega\mu_0\left(\bar{\bar{\mathbf{I}}}_t - \frac{\nabla_t\nabla_t'}{k_0^2}\right) \cdot (G_0(\mathbf{r} \mid \mathbf{r}') - G_0(\mathbf{r}_i \mid \mathbf{r}_i')) \tag{11}$$

where $G_0(\mathbf{r} \mid \mathbf{r}')$ is the free space Green's function

$$G_0(\mathbf{r} \mid \mathbf{r}') = \frac{e^{-jk_0|\mathbf{r}-\mathbf{r}'|}}{4\pi|\mathbf{r}-\mathbf{r}'|} \tag{12}$$

with the distance between source and test locations

$$|\mathbf{r}-\mathbf{r}'| = \sqrt{(x-x')^2 + (y-y')^2} \tag{13}$$

and the distance between source and test locations due to the image of the ground plane

$$|\mathbf{r}_i - \mathbf{r}_i'| = \sqrt{(x-x')^2 + (y-y')^2 + 4d^2}. \tag{14}$$

When the test location equals the source location, $x = x'$ and $y = y'$, the Green's function exhibits a strong singularity. A singularity of this order can cause severe numerical error when trying to numerically integrate such a function. For this reason it is desirable to work in the spectral domain. The spectral domain Green's functions are [13]

$$\tilde{G}_{Eh}^{xx}(k_x, k_y) = \frac{-Z_0}{2k_0}\left(\frac{k_0^2 - k_x^2}{k_z}\right)\left(1 - e^{-j2dk_z}\right) \tag{15}$$

$$\tilde{G}_{Eh}^{yy}(k_x, k_y) = \frac{-Z_0}{2k_0}\left(\frac{k_0^2 - k_y^2}{k_z}\right)\left(1 - e^{-j2dk_z}\right) \tag{16}$$

and

$$\tilde{G}_{Eh}^{xy}(k_x, k_y) = \tilde{G}_{Eh}^{yx}(k_x, k_y) = \frac{Z_0}{2k_0}\left(\frac{k_xk_y}{k_z}\right)\left(1 - e^{-j2dk_z}\right) \tag{17}$$

where

$$k_z^2 = k_0^2 - k_x^2 - k_y^2, \quad \mathrm{Im}(k_z) < 0. \tag{18}$$

III. Method of Moments

A. General Formulation

The boundary value problem for the current distribution on the planar radiating elements in the quasi-optical system is formulated as an electric field integral equation (EFIE). From the boundary condition stating that the total tangential electric field on the antenna surface is zero

$$-\mathbf{E}_t^{\mathrm{scat}}(x, y) = \mathbf{E}_t^{\mathrm{inc}}(x, y) \tag{19}$$

where subscript t denotes the tangential components of the electric fields. $\mathbf{E}_t^{\mathrm{inc}}$ is the incident electric field and $\mathbf{E}_t^{\mathrm{scat}}$ is the scattered electric field. The incident field is the electric field produced by the source that is used to excite the antenna surface. The incident field $\mathbf{E}_t^{\mathrm{inc}}$ produces a surface current density $\mathbf{J}_S$ on the patch surface which in turn produces a scattered field $\mathbf{E}_t^{\mathrm{scat}}$ where some of the field is coupled into the quasi-optical system and the rest of the field is radiated out of the system. The scattered field can be written in terms of a dyadic Green's function

$$\mathbf{E}_t^{\mathrm{scat}}(x, y) = \int_{y'}\int_{x'} \bar{\bar{\mathbf{G}}}_E \cdot \mathbf{J}_S(x', y')\, dx'dy'. \tag{20}$$

In order to solve for $\mathbf{E}_t^{\mathrm{scat}}$ in (20) an approximation for the unknown surface current density is needed. The unknown surface current density can be expanded in a set of N basis functions

$$\mathbf{J}_S(x', y') = \sum_{i=1}^{N} I_i\mathbf{W}_i(x', y') \tag{21}$$

where $\mathbf{W}_i$ is the ith basis function and I_i is its unknown complex amplitude. The basis functions $\mathbf{W}_i$ can represent currents in the x and y directions

$$\mathbf{W}_i(x', y') = W_i^x(x')\hat{\mathbf{a}}_x + W_i^y(y')\hat{\mathbf{a}}_y. \tag{22}$$

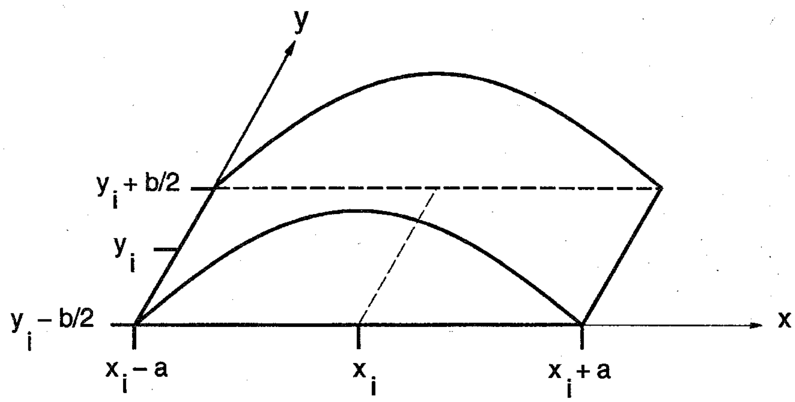

Fig. 3. An x-directed sinusoidal basis function.

Substituting (21) into (20) and testing (19) with the same set of basis functions, known as the Galerkin method, yields a set of linear algebraic equations to be solved for the unknown currents I_i

$$[\mathbf{Z}][\mathbf{I}] = [\mathbf{V}] \tag{23}$$

where the elements of the Z matrix are

$$Z_{ji} = -\int_y \int_x \int_{y'} \int_{x'} \mathbf{W}_j(x, y) \cdot \bar{\bar{\mathbf{G}}}_E \cdot \mathbf{W}_i(x', y')\, dx' dy' dx\, dy \tag{24}$$

and the elements of V are

$$V_j = \int_y \int_x \mathbf{W}_j(x, y) \cdot \mathbf{E}_t^{\mathrm{inc}}(x, y)\, dx\, dy. \tag{25}$$

B. Open Cavity Resonator

With the dyadic Green's function for the open cavity resonator being comprised of cavity and half-space contributions, it is best to work with the moment matrix elements in the same manner

$$Z_{ji} = Z_{c,ji} + Z_{h,ji} \tag{26}$$

where Z_c and Z_h represent the cavity and half-space contributions, respectively, with elements given by

$$Z_{c,ji} = -\int_y \int_x \int_{y'} \int_{x'} \mathbf{W}_j(x, y) \cdot \bar{\bar{\mathbf{G}}}_{Ec}(x, y; x', y') \cdot \mathbf{W}_i(x', y')\, dx' dy' dx\, dy \tag{27}$$

and

$$Z_{h,ji} = -\int_y \int_x \int_{y'} \int_{x'} \mathbf{W}_j(x, y) \cdot \bar{\bar{\mathbf{G}}}_{Eh}(x \mid x'; y \mid y') \cdot \mathbf{W}_i(x', y')\, dx' dy' dx\, dy. \tag{28}$$

It is important to note that $\bar{\bar{\mathbf{G}}}_{Ec}$ in (27) is not a function of the distance between the source and test location whereas $\bar{\bar{\mathbf{G}}}_{Eh}$ in (28) is a function of this distance. The final set of linear equations when solving for the x and y currents becomes

$$\begin{pmatrix} [Z_{ji}^{xx}] & [Z_{jk}^{xy}] \\ [Z_{li}^{yx}] & [Z_{lk}^{yy}] \end{pmatrix} \begin{pmatrix} [I_i^x] \\ [I_k^y] \end{pmatrix} = \begin{pmatrix} [V_j^x] \\ [V_l^y] \end{pmatrix} \tag{29}$$

where $Z_{ji}^{xx} = Z_{c,ji}^{xx} + Z_{h,ji}^{xx}$, $Z_{jk}^{xy} = Z_{h,jk}^{xy}$, $Z_{li}^{yx} = Z_{h,li}^{yx}$, $Z_{lk}^{yy} = Z_{c,lk}^{yy} + Z_{h,lk}^{yy}$, $j, i = 1, 2, \ldots, N_x$ and $l, k = N_x + 1, N_x + 2, \ldots, N$ with $N = N_x + N_y$. N_x and N_y are the number of x- and y-directed basis functions, respectively. The submatrix $[Z_{ts}^{vu}]$ denotes the contribution of v-directed testing of the field produced by u-directed current basis elements and the subscripts t and s refer to the individual test and source basis elements, respectively. The voltage vectors $[V_j^x]$ and $[V_l^y]$, of length N_x and N_y, respectively, correspond to x- and y-directed testing of the incident field. Similarly, $[I_i^x]$ and $[I_k^y]$ refer to the current expansion coefficients associated with each source basis function. The moment matrix $[\mathbf{Z}]$ is a square matrix of order N which is symmetrical (due to the Galerkin method) and diagonally strong.

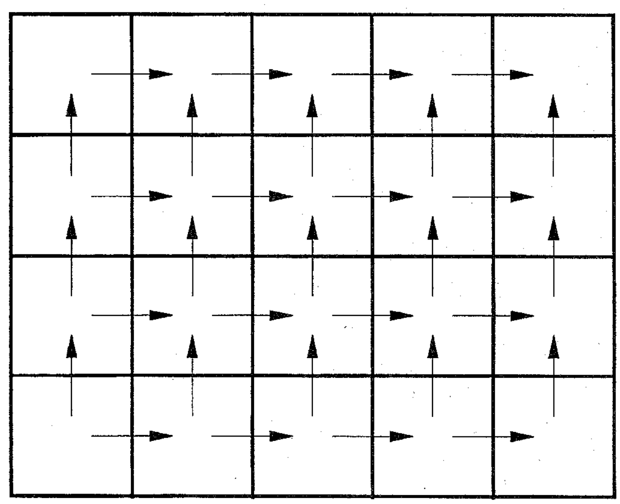

Fig. 4. Locations of x- and y-directed currents on a rectangular grid.

Sinusoidal basis functions are used for the current expansion and testing functions. An x-directed sinusoidal basis function centered at (x_i, y_i) is shown in Fig. 3 for a cell size of $a \times b$ and is given by

$$W_i^x(x) = \begin{cases} \dfrac{\sin[k_0(a - |x - x_i|)]}{b \sin(k_0 a)}, & |x - x_i| \le a \\ & |y - y_i| \le b/2 \\ 0, & \text{otherwise} \end{cases} \tag{30}$$

and for a y-directed sinusoidal basis function

$$W_i^y(y) = \begin{cases} \dfrac{\sin[k_0(b - |y - y_i|)]}{a \sin(k_0 b)}, & |y - y_i| \le b \\ & |x - x_i| \le a/2 \\ 0, & \text{otherwise.} \end{cases} \tag{31}$$

A basis function is spanned over two rectangular cells and the current amplitudes I_i are computed at the peak of each basis function as shown in Fig. 4.

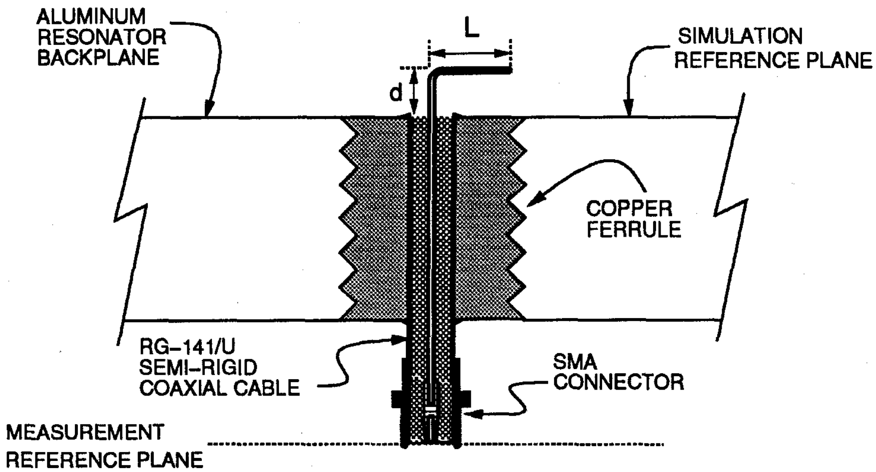

Fig. 5. A coaxial fed inverted L antenna.

For a grid divided into equal size rectangular cells of dimension $a \times b$, the moment matrix elements for the cavity contribution are found by substituting the Green's function given in (4) into (27) yielding

$$\begin{aligned} Z_{c,ji}^{xx} = & \sum_{m=0}^{N_m} \sum_{n=0}^{N_n} \frac{R_{mn}\psi_{mn}}{2(1+R_{mn}\psi_{mn})} \\ & \cdot \int_{y_i-\frac{b}{2}}^{y_i+\frac{b}{2}} \int_{x_i-a}^{x_i+a} W_i^x(x') \\ & \cdot \left[E_{mn}^-(x',y',d) - E_{mn}^+(x',y',d)\right] dx'dy' \\ & \cdot \int_{y_j-\frac{b}{2}}^{y_j+\frac{b}{2}} \int_{x_j-a}^{x_j+a} W_j^x(x) \\ & \cdot \left[E_{mn}^-(x,y,d) - E_{mn}^+(x,y,d)\right] dx\, dy \end{aligned} \tag{32}$$

and

$$\begin{aligned} Z_{c,lk}^{yy} = & \sum_{m=0}^{N_m} \sum_{n=0}^{N_n} \frac{R_{mn}\psi_{mn}}{2(1+R_{mn}\psi_{mn})} \\ & \cdot \int_{y_k-b}^{y_k+b} \int_{x_k-\frac{a}{2}}^{x_k+\frac{a}{2}} W_k^y(y') \\ & \cdot \left[E_{mn}^-(x',y',d) - E_{mn}^+(x',y',d)\right] dx'dy' \\ & \cdot \int_{y_l-b}^{y_l+b} \int_{x_l-\frac{a}{2}}^{x_l+\frac{a}{2}} W_l^y(y) \\ & \cdot \left[E_{mn}^-(x,y,d) - E_{mn}^+(x,y,d)\right] dx\, dy. \end{aligned} \tag{33}$$

The elements are calculated on the plane $z = d$ and contain no cross-terms. Since the Green's function given in (4) is a function of the source and test location and not the distance between the two, the four dimensional integration can be divided into two separate double integrations over the source and test fields. The double integration can be computed very efficiently and has no convergence problems. Since the elements are a sum of all the modes being considered, it is most efficient to combine separate computations of the double integration for each mode.

The moment matrix elements for the half-space having equal size cells of dimension $a \times b$ are found from (28) as

$$\begin{aligned} Z_{h,ji}^{xx} = & -\int_{y_j-\frac{b}{2}}^{y_j+\frac{b}{2}} \int_{x_j-a}^{x_j+a} \int_{y_i-\frac{b}{2}}^{y_i+\frac{b}{2}} \int_{x_i-a}^{x_i+a} G_{Eh}^{xx}(x \mid x'; y \mid y') \\ & \cdot W_j^x(x) W_i^x(x')\, dx'dy'dx\, dy \end{aligned} \tag{34}$$

$$\begin{aligned} Z_{h,jk}^{xy} = & -\int_{y_j-\frac{b}{2}}^{y_j+\frac{b}{2}} \int_{x_j-a}^{x_j+a} \int_{y_k-b}^{y_k+b} \int_{x_k-\frac{a}{2}}^{x_k+\frac{a}{2}} G_{Eh}^{xy}(x \mid x'; y \mid y') \\ & \cdot W_j^x(x) W_k^y(y')\, dx'dy'dx\, dy \end{aligned} \tag{35}$$

$$\begin{aligned} Z_{h,li}^{yx} = & -\int_{y_l-b}^{y_l+b} \int_{x_l-\frac{a}{2}}^{x_l+\frac{a}{2}} \int_{y_i-\frac{b}{2}}^{y_i+\frac{b}{2}} \int_{x_i-a}^{x_i+a} G_{Eh}^{yx}(x \mid x'; y \mid y') \\ & \cdot W_l^y(y) W_i^x(x')\, dx'dy'dx\, dy. \end{aligned} \tag{36}$$

and

$$\begin{aligned} Z_{h,lk}^{yy} = & -\int_{y_l-b}^{y_l+b} \int_{x_l-\frac{a}{2}}^{x_l+\frac{a}{2}} \int_{y_k-b}^{y_k+b} \int_{x_k-\frac{a}{2}}^{x_k+\frac{a}{2}} G_{Eh}^{yy}(x \mid x'; y \mid y') \\ & \cdot W_l^y(y) W_k^y(y')\, dx'dy'dx\, dy. \end{aligned} \tag{37}$$

As mentioned earlier direct evaluation of (34) and (37) would be very difficult due to the singularity that occurs when the source and test location are at the same point (self-term). The self-terms are the dominate terms in the moment matrix and inaccurate evaluation of these terms will result in unreliable solutions. For the cross terms (35) and (36) no singularity occurs because the source and test fields are never at the same location, but direct evaluation is still difficult due to the four integrations required. With these problems it is best to work in the spectral domain.

The dyadic Green's function for the half-space can be written as the inverse Fourier transform of

$$\begin{aligned} \bar{\bar{\mathbf{G}}}_{Eh}(x \mid x'; y \mid y') = & \frac{1}{4\pi^2} \int_{-\infty}^{\infty} \int_{-\infty}^{\infty} \tilde{\bar{\bar{\mathbf{G}}}}_{Eh}(k_x, k_y) \\ & \cdot e^{jk_x(x-x')} e^{jk_y(y-y')}\, dk_x\, dk_y. \end{aligned} \tag{38}$$

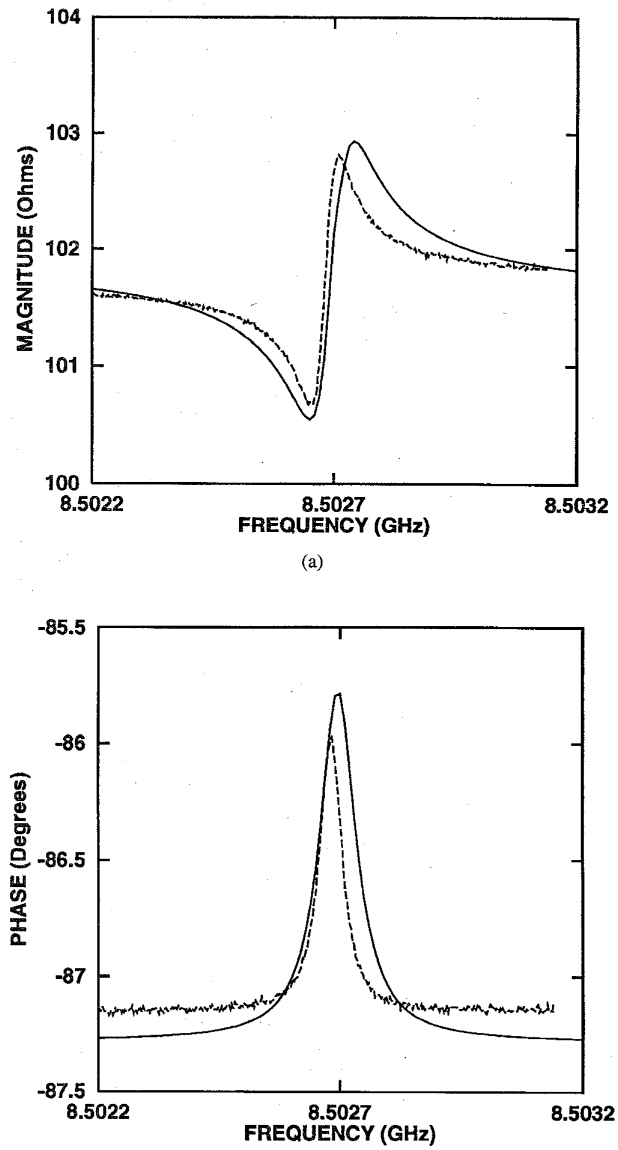

Fig. 6. Driving point impedance of the inverted L antenna for the $\mathrm{TEM}_{0,0,35}$ mode. (a) Magnitude. (b) Phase. Solid line, simulation; dashed line, measurement.

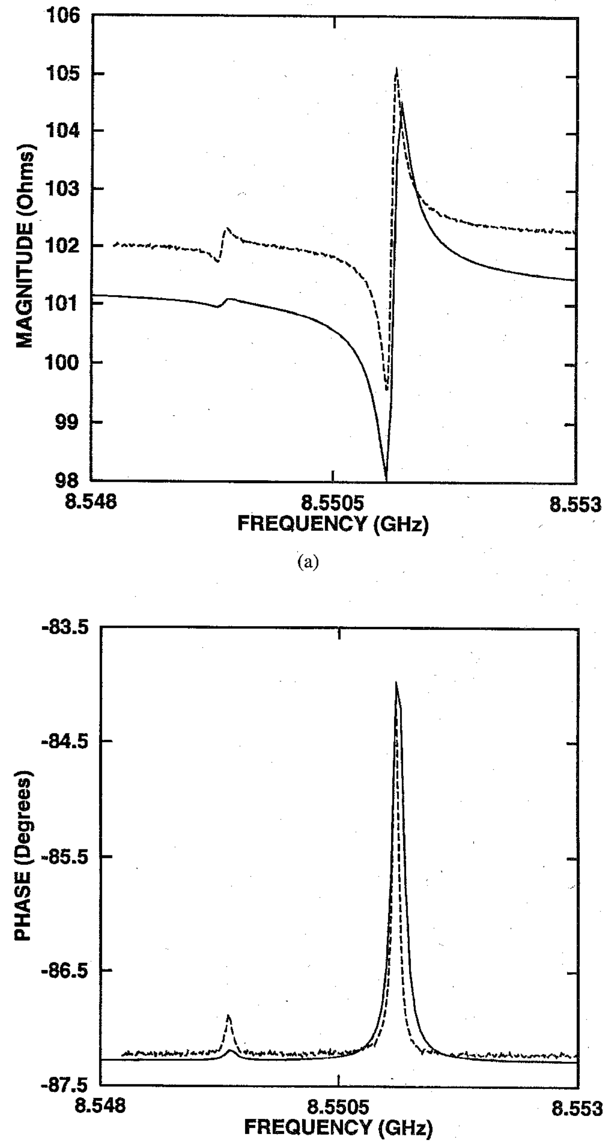

Fig. 7. Driving point impedance of the inverted L antenna for the $\mathrm{TEM}_{0,1,35}$ and $\mathrm{TEM}_{1,0,35}$ modes: (a) magnitude; (b) phase. Solid line, simulation; dashed line, measurement.

Applying (38) to (34)–(37) and using the even and odd properties of the integrands along with a transformation to polar coordinates, $k_x = \beta\cos\alpha$ and $k_y = \beta\sin\alpha$, results in the following

$$Z^{xx}_{h,ji} = \frac{-1}{\pi^2}\int_0^{\pi/2}\int_0^{\infty}\tilde{G}^{xx}_{Eh}(k_x,k_y) \cdot F^{xx}_{ji}(k_x,k_y)\,\beta\,d\beta\,d\alpha \tag{39}$$

$$Z^{yy}_{h,lk} = \frac{-1}{\pi^2}\int_0^{\pi/2}\int_0^{\infty}\tilde{G}^{yy}_{Eh}(k_x,k_y) \cdot F^{yy}_{lk}(k_x,k_y)\,\beta\,d\beta\,d\alpha \tag{40}$$

$$Z^{xy}_{h,jk} = Z^{yx}_{h,il} = \frac{-1}{\pi^2}\int_0^{\pi/2}\int_0^{\infty}\tilde{G}^{xy}_{Eh}(k_x,k_y) \cdot F^{xy}_{jk}(k_x,k_y)\,\beta\,d\beta\,d\alpha \tag{41}$$

where

$$F^{xx}_{ji}(k_x,k_y) = \cos\left[k_x(x_j - x_i)\right]\cos\left[k_y(y_j - y_i)\right] \cdot \left(\frac{2k_0}{\sin(k_0 a)}\right)^2\left[\frac{\sin(k_y b/2)}{(k_y b/2)}\right]^2 \cdot \left(\frac{\cos(k_x a) - \cos(k_0 a)}{k_0^2 - k_x^2}\right)^2 \tag{42}$$

$$F^{yy}_{lk}(k_x,k_y) = \cos\left[k_x(x_l - x_k)\right]\cos\left[k_y(y_l - y_k)\right] \cdot \left(\frac{2k_0}{\sin(k_0 b)}\right)^2\left[\frac{\sin(k_x a/2)}{(k_x a/2)}\right]^2 \cdot \left(\frac{\cos(k_y b) - \cos(k_0 b)}{k_0^2 - k_y^2}\right)^2 \tag{43}$$

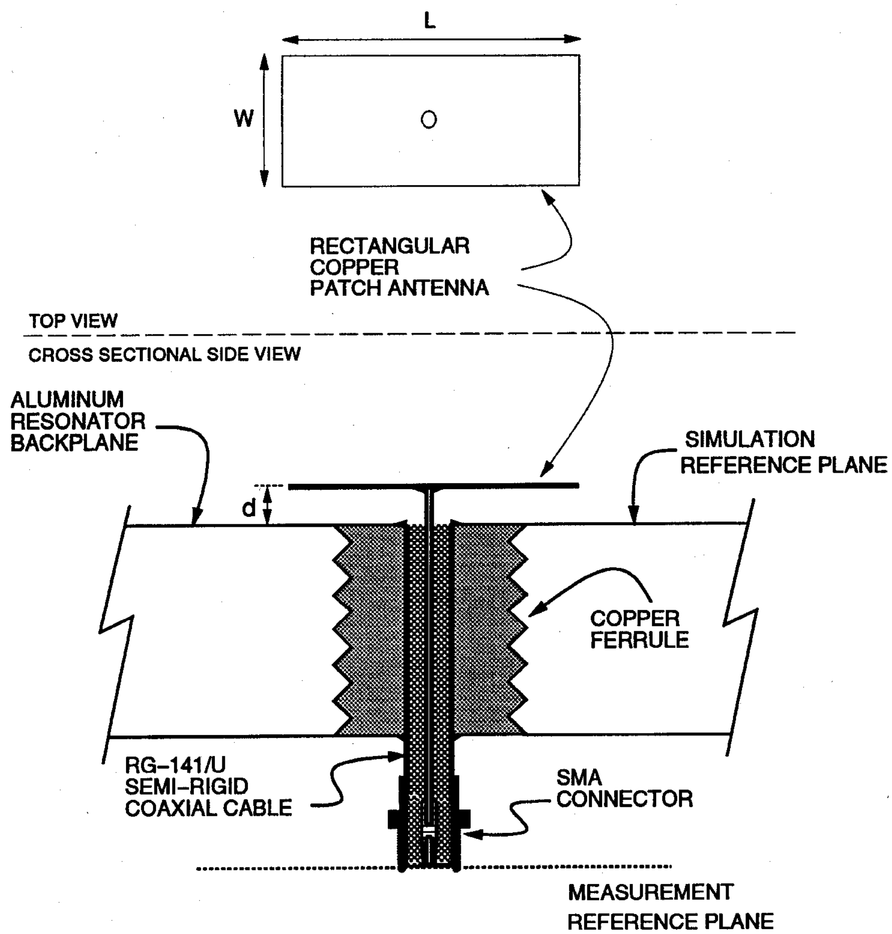

Fig. 8. A coaxial fed rectangular patch antenna.

$$\begin{aligned} F_{jk}^{xy}(k_x, k_y) = {} & \sin\left[k_x(x_j - x_k)\right] \sin\left[k_y(y_j - y_k)\right] \\ & \cdot \left(\frac{-4k_0^2}{\sin(k_0 a)\sin(k_0 b)} \right) \\ & \cdot \left[\frac{\sin(k_x a/2)}{(k_x a/2)} \right] \left[\frac{\sin(k_y b/2)}{(k_y b/2)} \right] \\ & \cdot \left(\frac{\cos(k_x a) - \cos(k_0 a)}{k_0^2 - k_x^2} \right) \\ & \cdot \left(\frac{\cos(k_y b) - \cos(k_0 b)}{k_0^2 - k_y^2} \right). \end{aligned} \tag{44}$$

The expressions in (42)–(44) are the results of the Fourier transforms of the basis functions evaluated in closed form. Techniques for efficient evaluation of the integrals in (39)–(41) can be found in [14], [15].

The excitation vector used for (25) is a delta-gap voltage generator given as

$$V_p = \begin{cases} 1 & \text{for } p \text{ equal to feed point} \\ 0 & \text{otherwise.} \end{cases} \tag{45}$$

The driving point impedance at the location of the delta-gap voltage generator is computed as

$$Z_{in} = \frac{V_p}{I_p} \tag{46}$$

where I_p is the current at the delta-gap computed by the method of moments.

IV. Comparison of Computed and Experimental Results

A. Inverted L Antenna

Comparisons of measured and simulated results were made for the open cavity structure shown in Fig. 1 with an electrically short inverted L antenna, shown in Fig. 5. The radii of focal lengths of the spherical reflector are $F_x = 0.894\,308$ m, $F_y = 0.953\,839$ m and $D = 0.620\,494$ m as determined in [2] and for the antenna the wire diameter is 0.9 mm and length L is 2.6 mm located at the planar reflector. The simulated results are virtually identical to those in [2]. Note that the previous work [2] is restricted to short wire antennas. For the simulation the L antenna was divided into 10 cells with a delta-gap source

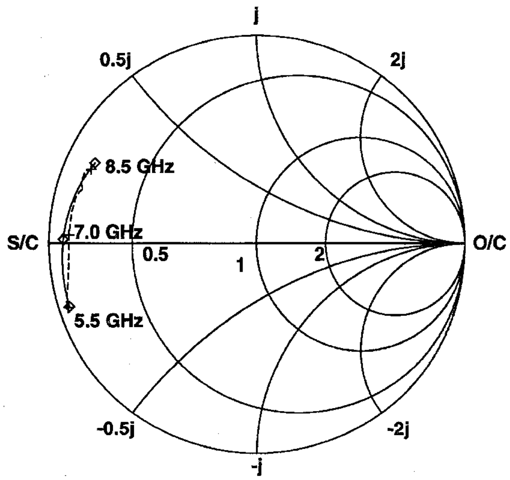

Fig. 9. Impedance Smith chart showing the driving point impedance of the patch antenna without the reflector: solid line, simulation; dashed line, measurement.

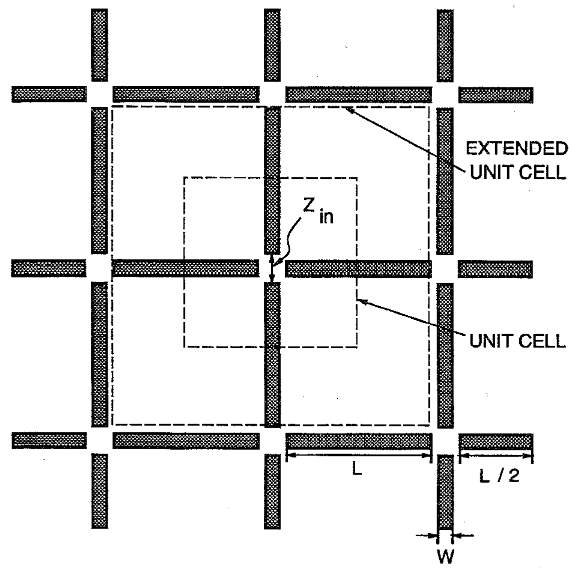

Fig. 10. A 3×3 grid in free space with the driving point impedance being measured in the middle gap.

placed between the first and second cells. The location of the antenna in the cavity was at (−90.6 mm, 15 mm) with $d = 1.9$ mm. The magnitude and phase of the driving point impedance are shown in Fig. 6 for the $\mathrm{TEM}_{0,0,35}$ mode and in Fig. 7 for the $\mathrm{TEM}_{0,1,35}$ and $\mathrm{TEM}_{1,0,35}$ modes (the $\mathrm{TEM}_{0,1,35}$ mode occurs first in frequency and then the $\mathrm{TEM}_{1,0,35}$ mode.)

B. Rectangular Patch Antenna

A measurement of a coaxial center fed rectangular patch antenna, shown in Fig. 8 with dimension $L = 15$ mm, $W = 5$ mm, and $d = 1$ mm, was taken without the reflector. The driving point impedance is shown in Fig. 9. Here the patch was divided into 16 cells with a delta-gap source placed in the center.

C. 3 × 3 Grid in Free Space

Measurements and simulations were performed in free space for the 3×3 grid shown in Fig. 10. The grid consists of 9 unit cells where each unit cell is of dimension 51.8 mm × 51.8 mm with the metallic grid lines having a length of $L = 42$ mm and a width of $W = 6.35$ mm. The gap spacing where the active device would be was 9.8 mm. Fig. 11 shows the driving point reflection coefficient magnitude for an extended unit cell (93.8 mm × 93.8 mm) with the same grid line width and gap spacing. Next the whole 3×3 grid structure was considered. Fig. 12 shows the driving point reflection coefficient magnitude in the center gap for the entire grid. From these results we can observe that there is significant mutual coupling between the grid elements. Measurements and simulations were also performed for the other gaps in the grid. The results indicate that the impedance for edge and corner gaps differs from that of the middle gap due to the finite extent of the grid. The technique presented here can calculate coupling parameters and location specific impedances which cannot be obtained using a unit cell approach.

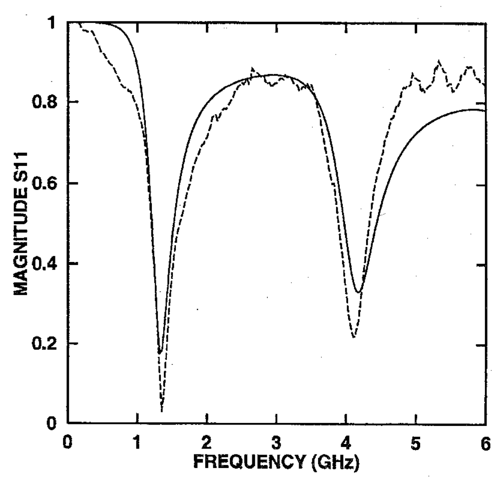

Fig. 11. Driving point reflection coefficient magnitude of the unit cell: solid line, simulation; dashed line, measurement.

V. Conclusion

A full-wave moment method implementation has been developed for the analysis of quasi-optical systems. This technique uses a dyadic Green's function which is derived by separately considering the paraxial and nonparaxial fields. This form of the dyadic Green's function is particularly convenient for quasi-optical systems because of its relative ease of development. This leads to computation of the moment matrix elements using a combination of spatial and spectral domains. Two types of quasi-optical systems were analyzed: the open cavity resonator, free space patch antenna resonator, and the grid radiator, where the radiating elements in each system were of finite size making no unit cell approximations. As a verification of the moment method, simulated results have been shown to compare favorably with measurements. The

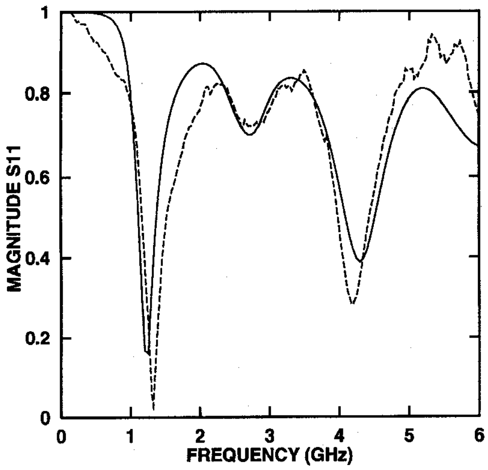

Fig. 12. Driving point reflection coefficient magnitude of the 3 × 3 grid: solid line, simulation; dashed line, measurement.

technique presented here will aid in the design of quasi-optical systems by accurately predicting the driving point impedances of the radiating elements.

References

[1] J. W. Mink, "Quasi-optical power combining of solid-state millimeter-wave sources," *IEEE Trans. Microwave Theory Tech.*, vol. MTT-34, pp. 273–279, Feb. 1986.

[2] P. L. Heron, G. P. Monahan, J. W. Mink, F. K. Schwering, and M. B. Steer, "Impedance matrix of an antenna array in a quasi-optical resonator," *IEEE Trans. Microwave Theory Tech.*, vol. 41, pp. 1816–1826, Oct. 1993.

[3] P. L. Heron, F. K. Schwering, G. P. Monahan, J. W. Mink, and M. B. Steer, "A dyadic Green's function for the plano-concave quasi-optical resonator," *IEEE Microwave Guided Wave Lett.*, vol. 3, pp. 256–258, Aug. 1993.

[4] P. L. Heron, "Modeling and simulation of coupling structures for quasi-optical systems," Ph.D. dissertation, North Carolina State Univ., 1993.

[5] K. Naishadham and T. W. Nuteson, "Efficient analysis of passive microstrip elements in MMIC's," *Int. J. Microwave and Millimeter-Wave Computer-Aided Eng.*, vol. 4, pp. 219–229, Mar. 1994.

[6] T. W. Nuteson, K. Naishadham, and R. Mittra, "Spatial interpolation of the moment matrix for efficient analysis of microstrip circuits," in *IEEE MTT-S Int. Microwave Symp. Dig.*, June 1993, pp. 971–974.

[7] R. M. Weikle II, M. Kim, J. B. Hacker, M. P. De Lisio, and D. B. Rutledge, "Planar MESFET grid oscillators using gate feedback," *IEEE Trans. Microwave Theory Tech.*, vol. 40, pp. 1997–2003, Nov. 1992.

[8] S. C. Bundy and Z. B. Popović, "A generalized analysis for grid oscillator design," *IEEE Trans. Microwave Theory Tech.*, vol. 42, pp. 2486–2491, Dec. 1994.

[9] T. W. Nuteson, G. P. Monahan, M. B. Steer, K. Naishadham, J. W. Mink, and F. K. Schwering, "Use of the moment method and dyadic Green's functions in the analysis of quasi-optical structures," in *IEEE MTT-S Int. Microwave Symp. Dig.*, May 1995, pp. 913–916.

[10] G. Goubau, "Beam waveguides," in *Advances in Microwaves*, vol. 3. New York: Academic, 1968, pp. 67–126.

[11] M. Abramowitz and I. Stegun, *Handbook of Mathematical Functions*. New York: Dover, 1972.

[12] C. Tai, *Dyadic Green's Functions in Electromagnetic Theory*, 2nd ed. New York: IEEE Press, 1994.

[13] D. M. Pozar, "Analysis and design considerations for printed phased-array antennas," in *Handbook of Microstrip Antennas*, J. R. James and P. S. Hall, Eds. London: Peter Peregrinus Ltd., 1989, pp. 693–753.

[14] ——, "Improved computational efficiency for the moment method solution of printed dipoles and patches," *Electromagnetics*, vol. 3, pp. 299–309, 1983.

[15] H. Y. Yang, A. Nakatani, and J. A. Castañeda, "Efficient evaluation of spectral integrals in the moment method solution of microstrip antennas and circuits," *IEEE Trans. Antennas Propagat.*, vol. 38, pp. 1127–1130, July 1990.

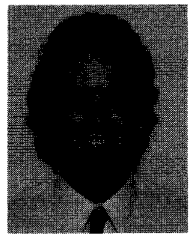

Todd W. Nuteson (S'90) was born in Tacoma, Washington, on November 16, 1967. He received the B.S. and M.S. degrees from Wright State University, Dayton, Ohio, both in electrical engineering, in 1991 and 1993, respectively. He is currently working toward the Ph.D. degree in electrical engineering at North Carolina State University.

From 1991 to 1993 he worked at Wright State University as a Research and Teaching Assistant. He received AFOSR Graduate Research Fellowships in 1992 and 1993. He holds a Research Assistantship with the Electronics Research Laboratory in the Department of Electrical and Computer Engineering. His research interests include numerical modeling of microwave and millimeter-wave circuits, quasi-optical power combining, antennas, and electromagnetics.

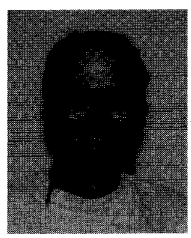

Gregory P. Monahan (M'95) received the B.S. degree in electrical engineering from the University of Maryland, College Park in 1967, the M.E. degree in electrical engineering from the University of Virginia, Charlottesville in 1989, and the Ph.D. degree from North Carolina State University, Raleigh in 1995.

From 1967 to 1971 he worked for the U.S. Naval Oceanographic Office in the areas of electronic navigation and data acquisition. From 1971 to 1986 he worked in the construction industry as manager of a general contracting construction company in Rappahannock County, VA. From 1983 to 1986 he was Business Manager for Wakefield School, a K-12 private school in rural Virginia. He is currently a Consulting Engineer with a specialization in personal computer based instrumentation measurement, control and analysis systems and in the design and planning of semiconductor clean room facilities.

Dr. Monahan is a member of the American Society for Engineering Education and a member of Sigma Xi.

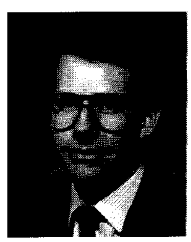

Michael B. Steer (S'77–M'83–SM'90) received the B.E. and the Ph.D. degrees in electrical engineering from the University of Queensland, Brisbane, Australia, in 1978 and 1983, respectively.

Currently he is Director of the Electronics Research Laboratory and Associate Professor of Electrical and Computer Engineering at North Carolina State University. His expertise in teaching and research involves circuit design methodology. From a teaching perspective he has taught courses at the sophomore through advanced graduate level in circuit design including basic circuit design, analog integrated circuit design, RF and microwave circuit design, solid state devices and computer aided circuit analysis. He teaches video-based courses on computer aided circuit analysis and on RF and microwave circuit design which are broadcast nationally by the National Technological University. His research has been directed at developing RF and microwave design methodologies. Currently his interests are in the computer aided engineering of quasi-optical power combining systems; the implementation of a two-dimensional quasi-optical power combining system; high efficiency, low cost RF technologies for wireless applications; and computer-aided engineering of mixed digital, analog and microwave circuits.

Dr. Steer is active in the Microwave Theory and Techniques (MTT) Society. In the MTT Society he serves on the technical committees on Field Theory and on Computer-Aided Design. He has organized many workshops and taught many short courses on signal integrity, wireless, and RF design. He is a 1987 Presidential Young Investigator and he has authored or co-authored more than 110 papers on topics related to RF and microwave design methodology. He has worked on projects sponsored by the National Science Foundation, the Army Research Office, SEMATECH, Airforce Office of Scientific Research, Advanced Research Projects Agency, BNR, DEC, IBM, Analog Devices, Compact Software, and Scientific Research Associates.

Krishna Naishadham, (S'83–M'86) photograph and biography not available at the time of publication.

James W. Mink (S'59–M'65–SM'81–F'91) received the Ph.D. degree from the University of Wisconsin in electrical engineering in 1964.

He joined North Carolina State University in 1994 on a full time basis where he is now a Visiting Professor and Graduate Coordinator in the Department of Electrical and Computer Engineering. His research focuses upon conformal antennas, in particular, wireless communications and millimeter-wave systems and devices. From 1976 through 1994, he was employed by the Army Research Office cumulating his service as the Director of the Electronics Division. From 1979 to 1994 he served as the principal Army representative of the Joint Services Electronics Program. Since 1987 he has served as a Program Evaluator for ABET and continues to serve in that capacity.

Dr. Mink is a member of the IEEE Antennas and Propagation Society Best Paper Awards from 1982 to the present. He served on the Centennial Medals Committee. He served as an Associate Editor for IEEE TRANSACTIONS ON ANTENNAS AND PROPAGATION from 1983 to 1989. He was Associate Editor of IEEE press book *Channel Characterization*. He was Guest Editor, IEEE-MTT special issues entitled "Quasi-Optical Techniques" and "Numerical Methods." He has published or presented about 60 refereed papers and he holds 5 patents. He was awarded the Superior Civilian Service Award for his program management achievements, a Bronze medal and two Research and Development Awards for technical achievements by the Department of the Army.

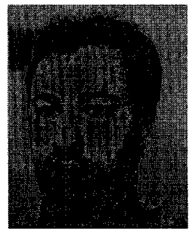

Konstantin K. Kojucharow was born in Eisleben, Germany, on January 27, 1970. He received the B.S. degree from the University of Technology in Dresden in 1992. He is currently working toward the M.S. degree.

In 1993 and 1994 as practical training he worked with the Technical Department of the German Aviation Administration on aeronavigational systems and later he worked with Mannesmann Mobilfunk, mobile telephone networks. He is currently working on the design of low-noise microwave amplifiers for portable communication systems. His research and work interests include microwave circuits, antennas, propagation, mobile communication systems, and radio/navigational systems.

James Harvey (M'91) received the B.S. degree in engineering from the United States Military Academy in 1964, the M.A. degree in physics from Dartmouth College in 1972, and the Ph.D. degree in applied science from the University of California at Davis, with research performed at Lawrence Livermore National Laboratory.

He is currently a Program Manager at the US Army Research Office, with primary responsibility for the fields of electromagnetics, millimeter wave circuit integration, low power/minimum power system design, and the electronic aspects of demining. His personal research interests are in the fields of quasi-optics and millimeter wave devices. He is active in the IEEE MTT Society, the IEEE LEO Society, URSI, and the American Physical Society.